NPS 61-87-004

NAVAL POSTGRADUATE SCHOOL

Monterey, California

CERENKOV AND SUB-CERENKOV RADIATION
FROM A CHARGED PARTICLE BEAM

By

J. R. NEIGHBOURS, F. R. BUSKIRK,
and X. K. MARUYAMA

3 March 1987

Technical Report

Approved for public release; distribution unlimited

Prepared for:
Defense Advanced Research Projects Agency
DARPA/STO
1400 Wilson Blvd.
Arlington, VA 22209

FedDocs
D 208.14/2
NPS-61-87-004

Fed Docs
D 208 14/2:
NPS-61-87-004

NAVAL POSTGRADUATE SCHOOL
Monterey, California

Rear Admiral R. C. Austin
Superintendent

D. A. Schrady
Provost

The work reported herein was supported by the Defense Advanced Research Projects Agency.

Reproduction of all or part of this report is authorized.

This report was prepared by:

Unclassified
URITY CLASSIFICATION OF THIS PAGE

DUDLEY KNOX LIBRARY
NAVAL POSTGRADUATE SCHOOL
MONTEREY CA 03943-5101

REPORT DOCUMENTATION PAGE

REPORT SECURITY CLASSIFICATION Unclassified	1b RESTRICTIVE MARKINGS
SECURITY CLASSIFICATION AUTHORITY	3. DISTRIBUTION / AVAILABILITY OF REPORT
DECLASSIFICATION / DOWNGRADING SCHEDULE	
ERFORMING ORGANIZATION REPORT NUMBER(S) PS 61-87-004	5. MONITORING ORGANIZATION REPORT NUMBER(S)
AME OF PERFORMING ORGANIZATION aval Postgraduate School	6b. OFFICE SYMBOL (*If applicable*) 7a. NAME OF MONITORING ORGANIZATION
DDRESS (*City, State, and ZIP Code*) onterey, CA 93943	7b. ADDRESS (*City, State, and ZIP Code*)
AME OF FUNDING / SPONSORING RGANIZATION Project Agency ense Advanced Research	8b. OFFICE SYMBOL (*If applicable*) 9. PROCUREMENT INSTRUMENT IDENTIFICATION NUMBER N6227186WR60058
DDRESS (*City, State, and ZIP Code*) PA/STO 0 Wilson Blvd., Arlington, VA 22209	10. SOURCE OF FUNDING NUMBERS PROGRAM ELEMENT NO. 62714E PROJECT NO. 6A10 TASK NO 5371/1 WORK UNIT ACCESSION NO.

ITLE (*Include Security Classification*)
Cerenkov and Sub-Cerenkov Radiation from a Charged Particle Beam

ERSONAL AUTHOR(S)
1st page

TYPE OF REPORT	13b. TIME COVERED	14. DATE OF REPORT (*Year, Month, Day*)	15. PAGE COUNT
nical	FROM Aug. 86 TO Mar 87	March 3, 1987	

UPPLEMENTARY NOTATION

COSATI CODES			18. SUBJECT TERMS (*Continue on reverse if necessary and identify by block number*)
IELD	GROUP	SUB-GROUP	

BSTRACT (*Continue on reverse if necessary and identify by block number*)

BSTRACT: As a consequence of the relaxation of the phasing condition between the oving charge and radiated wave for finite beam path lengths, the Cerenkov peak is roadened and the threshold energy is developed which is applicable to charged eams consisting of single point charge or charge bunch of finite size, as well as eams consisting of periodically repeated bunches.

STRIBUTION / AVAILABILITY OF ABSTRACT ☒ UNCLASSIFIED/UNLIMITED ☐ SAME AS RPT. ☐ DTIC USERS	21. ABSTRACT SECURITY CLASSIFICATION
AME OF RESPONSIBLE INDIVIDUAL	22b. TELEPHONE (*Include Area Code*) 22c. OFFICE SYMBOL

ORM 1473, 84 MAR 83 APR edition may be used until exhausted.
All other editions are obsolete

SECURITY CLASSIFICATION OF THIS PAGE

☆ U.S. Government Printing Office: 1986—606-24.

Cerenkov and Sub-Cerenkov Radiation from a Charged Particle Beam

John R. Neighbours

Fred R. Buskirk

Xavier K. Maruyama+

Physics Department

Naval Postgraduate School

Monterey, California 93943

ABSTRACT

As a consequence of the relaxation of the phasing condition between the moving charge and radiated wave for finite beam path lengths, the Cerenkov peak is broadened and the threshold energy is lowered. A criterion for the threshold energy is developed which is applicable to charged beams consisting of single point charge or charge bunch of finite size, as well as beams consisting of periodically repeated bunches.

+ Permanent Address - National Bureau of Standards, Gaithersburg, MD 20899

INTRODUCTION

In previous work[1] we have given a form for the Cerenkov radiation from periodic electron bunches propagating in a homogeneous medium. The method involved construction of the Fourier components of the field which in turn led to the Poynting vector expressed as harmonics of the basic electron beam frequency. The important results were that the Cerenkov cone angle is shifted substantially beyond the ordinary Cerenkov angle θ_c, ($\cos\theta_c = (n\beta)^{-1}$) and broadened so that a significant fraction of the power radiated appears at angles other than θ_c. As either frequency or the path length of the beam increases, the cone angle was found to approach θ_c with an increasing fraction of the total radiation being radiated at that angle.

In a second paper[2], we showed preliminary experimental data and the results of calculations for X and K band microwave Cerenkov radiation produced by the electron bunches from an S band 100 MeV Linac beam propagating in air. These results as well as other published[3] and unpublished ones are in substantial agreement with the predictions of reference 1.

Subsequently we discussed several aspects of the expected Cerenkov radiation from an intense electron beam[4], and the emission thresnold[5] for radiation in brief reports. The onset of Cerenkov radiation was ascribed to a relaxation of the phase matching condition between the charge and the wave and the effect has been investigated theoretically and experimentally in the optical region.[6,7,8]

Recently[9] we have corrected an error appearing in the appendix of reference 1 and have shown that the radiated energy from a single charge bunch has the same form as the radiated power from a beam of periodic bunches. Radiation from a periodic beam occurs at the fundamental frequency and harmonics, whereas radiation from a single charge bunch has a continuous frequency distribution.

The purposes of this paper are:

(1) to amplify our remarks concerning the effects of a finite electron beam path on the sharpness and intensity of the radiation pattern.

(2) to show in detail how the energy threshold for the onset of Cerenkov radiation is affected by the electron beam path path length.

CHARACTERISTICS OF COHERENT CERENKOV RADIATION

The total coherent power per unit solid angle, radiated at the frequency ν by a periodic charged particle beam in traveling a finite distance L at constant velocity is[2]

$$W(\nu,\vec{k}) = \nu_o^2 \, QR^2 \tag{1}$$

where ν_o is the fundamental frequency of the beam generator and ν is a harmonic of ν_o, q is the charge of an individual bunch, Q is a constant and R is the radiation function. The bunches in the beam are assumed to be rigid, i.e. unchanging in shape and size as the beam travels through the medium (usually air) at a velocity given by $v = \beta c_o$. The velocity of light in vacuum is c_o and the velocity of light in the medium is $c = c_o/n$ where n is the index of refraction.

Similarly, E, the energy radiated per unit solid angle within the frequency range $d\nu$ by a single bunch of charge q traveling a distance L is[9]

$$E(\nu,\vec{k})\, d\nu = QR^2 d\nu \tag{2}$$

In both cases the constant Q is

$$Q = \frac{\mu c q^2}{8\pi^2} \tag{3}$$

where μ is the permeability of the medium, and the radiation function R is given by

$$R = 2\pi\eta \sin\theta \, I(u) \, F(\vec{k}) \tag{4}$$

where θ is the angle between the direction of travel of the

charged particle beam and the direction of propagation of the emitted radiation, I(u) is the diffraction function, and $F(\vec{k})$ is the form factor. In the remainder of this paper we refer only to W although the discussion and results also apply to E, since W and E have the same spatial distribution.

It is convenient to measure the finite length of travel of the charged particle beam in units of the wavelength in the medium of the emitted radiation. Accordingly, the dimensionless beam length parameter η which appears in the radiation function explicitly, and implicitly as part of the diffraction parameter defined below, is defined as the ratio of the path length of the charged particle beam to the wavelength in the medium of the emitted radiation.

$$\eta = \frac{L}{\lambda} \tag{5}$$

The diffraction function is

$$I(u) = \frac{\sin u}{u} \tag{6}$$

where the dimensionless diffraction parameter u depends upon the Cerenkov angle given by $\cos\theta_c = (n\beta)^{-1}$, as well as upon the beam length parameter and the radiation emission angle.

$$u = \pi\eta[(n\beta)^{-1} - \cos\theta] \tag{7}$$

The wave vector of the emitted radiation is $\vec{k}$ ($k = \omega/c$), and $F(\vec{k})$ is the dimensionless form factor. That is, if $\rho(\vec{r})$ is the charge distribution of a single bunch, then the Fourier components of the charge are

$$\rho(\vec{k}) = \int_{-\infty}^{\infty}\int\int \rho(\vec{r})\, e^{i\vec{k}\cdot\vec{r}}\, d^3r \qquad (8)$$

and the form factor is defined by

$$\rho(\vec{k}) = q\, F(\vec{k}) \qquad (9)$$

For a point charge, $F(\vec{k})$ is identically one for all values of $\vec{k}$.

The actual radiator is the medium. Radiation is emitted in a cylindrically symmetric pattern about the length of the charged beam and with a transverse polarization lying in the plane of the beam and the direction of propagation of the radiation. Since R depends directly upon η, the strength of the radiation is proportional to the square of the path length of the beam.

When the wavelength of the emitted radiation is long compared to the dimensions of an individual charge bunch, $F(\vec{k})$ is slowly varying with angle so that the pattern of emitted radiation is dominated by the diffraction function, I(u). Regardless of the behaviour of $F(\vec{k})$, the radiation pattern has zeroes occuring for integral multiples of π. The largest value of $(I(u))^2$ occurs at $u = 0$ $(\theta=\theta_c)$ with subsidiary maxima at $u = 1.4303,\ 2.4590,\ 3.4709,\ 4.4774$ etc. The maxima of the radiation (W or E) are displaced from these values by the $(\sin\theta)^2$ factor, and by the relatively small variation of $(F(\vec{k}))^2$.

Formally, the diffraction function radiation pattern is similar to that resulting from diffraction by a single slit in which the incoming plane wave is highly oblique, or to an "end fire" antenna array. The actual radiation pattern is skewed from this by the variation of the $\sin\theta$ factor in R.

For short beam path lengths (small η), the principal and subsidiary radiation lobes are broad with maxima strongly influenced by the $(\sin\theta)^2$ factor. As η increases, all the radiation lobes increase in intensity with the principal lobe increasing most rapidly; concomitantly the lobes are displaced less from the maxima of $(I(u))^2$. In the limit of infinite beam path length, the only significant radiation arises from the principal lobe, which is centered on the Cerenkov angle.

In the regime where the radiation wavelength is much greater than the extent of the charge bunches, the variation of R with $F(\vec{k})$ can be neglected. In this case the position of the maxima can be found from the solution of the transcendental equation

$$\frac{\tan u}{u} = \left(1 - \frac{u}{\pi\eta}\,\frac{\cos\theta}{(\sin\theta)^2}\right)^{-1} \qquad (10)$$

where $\cos\theta$ is obtained from (7)

$$\cos\theta = \frac{1}{n\beta} - \frac{u}{\pi\eta} \qquad (11)$$

Equation (10) is expressed as an equation in u by substituting (11). After the value of u satisfying (10) is determined, the angular position of the maxima is found from (11). Then, the maximum value of the radiation function is found from (4).

Observation of the radiation patterns is difficult because of unwanted reflections from the ground plane and the walls of the experimental chamber. However, taking pains to eliminate extraneous signals leads to reasonably good agreement[3] between theory and experiment.

Fig. 1, similar to Fig. 4 and Fig. 5 of Reference 2, shows the fundamental (η=10) and first harmonic radiation patterns (η=20) calculated for an electron beam issuing from an S-band 100 Mev linac into air (n = 1.000268) where it travels 105 cm. The effects of changes in the beam length parameter, η, described above, are clearly evident in the figure. Fig. 2 calculated for larger values of η shows a continuation of the trend of the major radiation peak to narrow and grow in intensity as the beam length increases.

Although the above discussion is for the Cerenkov regime of radiation ($n\beta > 1$), there is no such restricting condition in the development leading to (1) and (2), and therefore these equations and their consequences are expected to hold for all possible values of $n\beta$. This leads to an apparent contradiction since it is well known from other calculations and experiments that in the sub-Cerenkov regime ($n\beta < 1$) the strength of the radiation does not depend on the path length of the charged particle beam. This point is addressed in a later section.

SHARPNESS OF THE MAIN CERENKOV RADIATION LOBE

It is difficult to deal analytically with the maxima of W even if $F(\vec{k})$ has a relatively simple form. But regardless of the exact shift of the maxima, the diffraction function always has zeroes at $u = m\pi$. The corresponding θ values are given by

$$\cos\theta_m = \frac{1}{n\beta} - \frac{m}{\eta} \tag{12}$$

where m is an integer. For $m = \pm 1$, these limits restrict the value of the principal peak of W to lie between the θ values determined by these zeroes in I(u); assuming that these values of u correspond to physical values of θ. Substituting $m = \pm 1$ into (12) gives

$$\cos\theta_a = (n\beta)^{-1} + \eta^{-1} \quad (m=-1) \tag{13}$$

$$\cos\theta_b = (n\beta)^{-1} - \eta^{-1} \quad (m=+1) \tag{14}$$

for the upper (θ_b) and lower (θ_a) bounds of the main peak.

The behavior of the main radiation lobe, bounded by the angles ϑ_b and ϑ_a, depends on the constants $n\beta$ and η. It is obvious that as $\eta \to \infty$, the lobe narrows and both θ_b and θ_a approach θ_c, assuming, of course, that $n\beta > 1$ and θ_c is defined. In this limit of an infinite medium, the radiation all appears at the Cerenkov angle.

In the other extreme, as η becomes smaller, diffraction spreads out the main lobe, and θ_b increases from θ_c to eventually become 180° for the value η_b of the beam length parameter, where

$$\eta_b = n\beta(n\beta + 1)^{-1} \tag{15}$$

For realizable values of $n\beta$, η_b has a value of approximately 1/2.

Similarly, as η decreases, θ_a diminishes and becomes zero for $\eta=\eta_a$, where

$$\eta_a = n\beta(n\beta-1)^{-1} \tag{16}$$

One notes that η_a is larger than η_b, and that η_a varies considerably depending on the value of $n\beta$. For realizable values of $n\beta$, η_a approaches 1; wheras for $n\beta$ only slightly greater than one, η_a is quite large. For example, 100 MeV electrons in air ($n\beta$ = 1.000255) have an η_a value of 3920 while the same electrons in water ($n\beta$=1.333) have an η_a value of 4.

For path lengths shorter than η_a only the upper bound has physical reality. This does not mean that a Cerenkov radiation peak does not occur for these short beam lengths, but only that the peak bound suggested by (13) is inapplicable and that the lower bound on the peak angle is zero.

Behaviour of the two angular bounds is shown in Fig. 3 for 100 MeV electron bunches from an S-band Linac propagating in air (θ_c = 1.3°) and water (θ_c = 41.4°). For both materials, the angular difference (θ_b - θ_a) is large for relatively short beam paths but as η increases, the difference diminishes and both radiation patterns approach a δ like function centered about θ_c.

As mentioned earlier, the main radiation peak is sensitive to the form factor so that it is difficult to determine θ_m, the value of θ for which the radiated power is a maximum, except by numerical studies. Fig. 3 also shows such numerical results for air, obtained from the calculations which led to Fig. 7 of Ref. 2. Taking the lower bound to be zero when θ_a does not exist, the graph shows that as a rule of thumb, θ_m occurs roughly midway

between the bounds θ_b and θ_a. As pointed out in Ref. 2, the spreading of the main lobe of radiation about θ_c is assymetric from the $\sin\theta$ factor in (4) so that θ_m is larger than θ_c.

EMISSION THRESHOLD

The above discussion showed that as η varies, the upper and lower bounds and therefore the peak between them can change position, and Fig. 3 shows the effects of varying path length at constant electron beam energy, i.e. as η increases, θ_b and θ_a, both move toward θ_c.

Both the beam length and the beam energy (through β) affect the position of θ_b and θ_a. At some finite η the radiation pattern is spread into a diffraction lobe bounded by θ_b and θ_a. As the beam energy, and thus β, is reduced, θ_b, θ_c, and θ_a become smaller. The angles may become non-physical because the governing equations contain cos θ which formally may exceed unity. Since the inequality $\theta_a < \theta_c < \theta_b$ is always satisfied, it is possible to have only θ_a be non-physical as discussed in the previous section, or to have both θ_a and θ_c non-physical. In either case, the resulting main lobe of radiation extends from zero degrees to θ_b and this phenomenon may be termed sub-Cerenkov radiation because it occurs for $n\beta$ less than (but usually close to) unity. More precise delineation of parameter ranges for $n\beta$ and η are discussed below. The spreading of the lobe and the conditions for sub-threshold Cerenkov radiation depend only on the parameter η, which depends on L and λ. The beam bunch size parameters enter only because long wave length Cerenkov radiation is strong only for bunched beams.

We define the onset or threshold of the emission of Cerenkov radiation to be the situation when θ_b begins to enter the

physical range. Then setting $\theta_b=0$ in (14) gives the threshold relation.

$$n\beta = \eta\,(\eta+1)^{-1} \tag{17}$$

A plot of (17) is shown in Fig. 4. As the path length increases, the product $n\beta$ first rises rapidly and then asympotically approaches the value unity. For values of $n\beta > 1$, the Cerenkov angle θ_c is in the physical range and diffracted Cerenkov radiation is emitted. For values of $n\beta$ and η between the curve and unity, θ_c is nonphysical but radiation with a well defined peak is still produced. For values of $n\beta$ and η below the curve, radiation is emitted with a rapidly oscillating spatial dependence. Although Fig. 4 is a universal curve, it is useful and instructive to construct threshold energy curves for particular materials.

Using the usual relation between β and γ, (17) can be written in terms of γ_t, the value of γ necessary for the onset of sub-Cerenkov radiation.

$$\gamma_t(\eta) = \left[1 - \frac{1}{n^2(1+\eta^{-1})^2}\right]^{-1/2} \tag{18}$$

This gives the required energy $E_t = \gamma_t E_o$ for the onset of emission in terms of the index of refraction n and the path length η. The energy required for onset of emission is then given by $E_t = \gamma_t E_o$.

Limiting values of (18) can be obtained for very long and very short path lengths. For infinite path length

$$\gamma_t(\eta=\infty) = \left[1 - \frac{1}{n^2}\right]^{-1/2} \qquad (19)$$

which is the same condition as $n\beta = 1$, the usual threshold for emission of Cerenkov radiaton. For large n, $\gamma_t(\eta=\infty)$ approaches the value of 1. If n~1 as for most gases, the threshold value of $\gamma_t(\eta=\infty)$ is large and depends critically on the particular value of n. Then, introducing the refractivity δ and writing the index of refraction as $n=1+\delta$, the threshold value of $\gamma_t(\eta=\infty)$ is proportional to $\delta^{-1/2}$; and in the limit of small δ

$$\gamma_t(\eta=\infty) \cong (2\delta)^{-1/2} \qquad (20)$$

From (20), the threshold energy at infinite beam length is 22.1 MeV for electrons in air and 60.2 MeV for electrons in helium.

For short path lengths, (18) shows that, as $\eta \to 0$, $\gamma_t(\eta=0) \to 1$ independent of the value of n. Thus for very short paths, there is no threshold. This may be seen from (17) where as $\eta \to 0$, the value of β at threshold also approaches zero.

Since many charged particle beams are composed of electrons, it is convenient to display threshold energy (instead of γ_t) as a function of beam length as is shown in Fig. 5. Plots for three materials with different indices are shown: all approach 0.511 MeV for short path lengths and approach the value given by (19) for long beam lengths.

From (19), the variation of the threshold emission energy of a medium with a large index of refraction is small. Thus for water, the emission threshold is relatively independent of particle beam path length, varying between 0.511 and .077 MeV.

For gases the variation is larger - over two decades in the case of helium.

This large variation in threshold energy with path length means that Cerenkov-like radiation can be produced by short beams with energies substantially below the threshold energy for infinite path length. For example, a 10 MeV electron beam with a length of $\eta = 10$ would be well above the threshold for either helium or air, but would be far below the infinite path length threshold values of 60.2 and 22.1 MeV. Such a beam would produce Cerenkov-like radiation in either medium.

Since the thresholds for the two gases are different for the larger path lengths, it is possible to find sets of parameters where one gas is favored. A beam with an energy of 18 MeV and a length parameter $\eta \sim 4 \times 10^3$ would produce Cerenkov-like radiation when propagating in air but not helium.

Fig. 3 shows how the width of the main lobe varies with the path length of 100 MeV electron bunches. For other beam energies above $E_t(\eta=\infty)$, the threshold curves for infinite path length are similar except displaced. As the beam energy decreases the Cerenkov angle θ_c which is the asymptote of the θ_b and θ_a curves, is lowered, and consequently it is approached at increasingly larger path lengths. For beam energies very close to $E_t = \gamma_t(\eta=\infty)E_o$ the asymptotic nature is not evident until extremely long path lengths are attained. (This behaviour is not surprising since at E_t the Cerenkov angle is zero at infinite path lengths).

The limits on path length for either Θ_a or Θ_b to be physical are obtained from (13) and (14) by setting the angle equal to zero. The limiting path length for Θ_a to be nonphysical is η_a as given by (16), and the approach of Θ_a to this limit for beam energies well above E_t is shown in Fig. 3. For Θ_b , the limiting value of path length denoted η_L, is

$$\eta_L = n\beta\,(1-n\beta)^{-1} \qquad (21)$$

which gives a non realistic (negative) value for beam energies above E_t and a positive value for energies below E_t.

Consequently the behaviour of curves like those in Fig. 3 is different for energies less than E_t. For these energies, (16) gives a negative result for η_a and therefore for these energies only Θ_b is physical, and only for path lengths <u>less</u> than η_L.

ENVELOPE OF THE RADIATION

The diffraction analysis of the radiation is correct in predicting the angular dependence and intensity of the radiation, and its variations with frequency, and path length of the charged particle beam. However, an understanding of the sub-Cerenkov radiation patterns and their development into the characteristic Cerenkov shape is more easily displayed with a different expression for the previous formulation.

Substituting for u in the diffraction function allows the radiation function to be written

$$R = 2\,\vec{F(k)}\,\sin u\;\; G(n\beta,\theta) \tag{22}$$

where $G(n\beta,\theta)$ is a function that often arises in radiation calculations,

$$G(n\beta,\theta) = \frac{\sin\theta}{(n\beta)^{-1}-\cos\theta} \tag{23}$$

Both the radiated power W and the radiated energy E are proportional to R^2, and the radiation patterns can be thought to be an oscillatory function modulated by an envelope. If variation of R with $\vec{F(k)}$ is neglected, then aside from some constants, $(G(n\beta,\theta))^2$ is the envelope of the oscillating $\sin^2 u$ function which takes on values between zero and one. The form of the envelope depends upon the value of $n\beta$. Either there is a peak at $\cos\theta_s = n\beta$, or there is a pole at $\cos\theta_c = 1/n\beta$; only one possibility is allowed. Regardless of the value of $n\beta$, the function has zeroes at $\theta=0$ and $\theta=\pi$.

Radiation is in the sub-Cerenkov regime when $n\beta<1$. Then the envelope function has a peak at θ_s ($\cos\theta_s=n\beta$) of height equal to ($\cot^2\theta_s$). In this case, the height of the peak does not depend upon the path length of the charged particle beam. Consequently, the largest possible value of the radiation function in the sub-Cerenkov case is

$$R^2(\theta_s) = 4\ F^2(\vec{k})\ \cot^2\theta_s \tag{24}$$

regardless of the length of the beam.

As $n\beta$ increases, the peak angle θ_s decreases and the height of the peak grows. When $n\beta=1$, the peak angle goes to zero, the envelope function has a pole (at $\theta=0$), and the Cerenkov regime is attained.

In the Cerenkov regime ($n\beta>1$) the envelope has a pole at the Cerenkov angle ($\cos\theta_c=1/n\beta$). However, since $\sin u$ is always zero at the Cerenkov angle, the radiation function remains finite, with a value of

$$R^2(\theta_c)=4\pi^2\eta^2F^2(\vec{k})\ \ \sin^2\theta_c \tag{25}$$

In the Cerenkov case, the height of the peak depends explicitly upon the value of the beam length.

Fig. 6 shows a plot of the envelope function for the two cases. For illustrative purposes the curves are drawn for a plus and minus two per cent variation from the Cerenkov threshold of $n\beta=1$. These values of $n\beta$ give $\theta_s=11.48$ degrees and $\theta_c=11.36$ degrees.

Since (7) shows that u is a function of θ, as θ varies from zero to π, u will go through many cycles, the exact number

depending on the value of the path length parameter η. Successive zeroes of $\sin^2 u$ will occur at integral multiples of π, with maximum values (of 1.0) cccurring halfway in between. The radiation pattern, proportional to the product of $\sin^2 u$ and $(G(n\beta,\theta))^2$ then will have zeroes and maxima at the corresponding theta values.

In the limit of very long beam path length, the $\sin^2 u$ function oscillates very rapidly causing the adjacent peaks to be very closely spaced in θ. This behavior can be seen by differentiating (7) to obtain

$$\delta u = \pi\eta \sin\theta \quad \delta\theta \tag{26}$$

The peaks of $(\sin^2 u)$ occur at intervals of π, and setting $\delta u = \pi$ gives

$$\delta\theta = (\eta \sin\theta)^{-1} \tag{27}$$

showing that the peak spacing becomes very small as η increases.

SUB CERENKOV RADIATION PATTERNS

To illustrate the development of the radiation patterns, consider the pattern formed with the sub-Cerenkov envelope in Fig 6, drawn for $n\beta=0.98$, corresponding to 2.55 MeV electrons traveling in air. Fig 7 shows the radiation patterns in the forward direction calculated for $n\beta=0.98$ and two different values of η. The envelope of the pattern is clearly evident for angles greater than approximately 20 degrees. Since the spacing of the oscillations is greater at lower angles the envelope is less evident at these angles. As the radiation angle increases to values larger than shown, both curves continue to have a monotonically decreasing set of peaks.

For $\eta=12$ the radiation has a single dominant peak and several subsidiary ones. For $\eta=37$ the largest peak is not the first, and there are several secondary peaks of approximately the same height; no single one being outstanding. If the beam path length is increased still farther, many closely spaced peaks appear inside the envelope, with no single peak being dominant. The radiation pattern begins to be rapidly oscillating as shown in Fig 8 for $\eta=100$.

Consequently, in the sub-Cerenkov case there are two types of radiation patterns; those without a single dominant peak, and those that have a dominant peak giving the appearance of diffracted Cerenkov radiation. The latter case we call psuedo-Cerenkov radiation.

The difference between sub-Cerenkov radiation patterns with a dominant peak and those with peaks of roughly the same size is

one of path length. When the oscillating $\sin^2 u$ function has a maxima near the maximum of the envelope function, that peak will be largest. The positions of the maxima in $\sin^2 u$ are found by setting u in (7) to be an odd multiple of $\pi/2$, giving

$$\cos\theta_p = \frac{1}{n\beta} - \frac{p}{2\eta} \tag{28}$$

where p is an odd integer. If these maxima are to occur at the peak of the envelope function, the angle given by (28) is equal to the peak angle θ_s. Substituting $\cos\theta_s = n\beta$ in (28) yields the condition that successsive maxima will occur at θ_s

$$\frac{p}{2\eta} = \frac{1 - (n\beta)^2}{n\beta} = \sin\theta_s \tan\theta_s \tag{29}$$

which shows that if p is incremented, η also must change in order to maintain a maxima at θ_s.

Fig 7 is calculated for p=1 (solid line) and p=3 (dashed line). The solid line shows a single dominant peak with a ratio of the height of the first to second peak of nearly two. This curve appears similar to the Cerenkov radiation patterns shown in Fig 1, and therefore is an example of psuedo-Cerenkov radiation. Since the lobes of the dashed curve are more closely spaced, this curve has a lower ratio of first to second peak heights and this pattern has begun to approach the rapidly oscillating behaviour region of Fig 8. For large values of p (and therefore η) the distinction of a maxima occurring at θ_s becomes less important, and these patterns become practically indistinguishable from patterns like that in Fig 8 which was calculated for an arbitrary value of η.

CERENKOV RADIATION PATTERNS

In the Cerenkov regime, development of the radiation pattern is calculated by methods similar to those employed in the previous section. The oscillating $\sin^2 u$ function is again modulated by the envelope function, Eq (23) which now has a singularity at θc. The position of the maxima of their product is displaced from θ_c and with a value different from (25). Because the envelope function is so strongly peaked in this case, there is always a single portion of the $\sin^2 u$ function that is greatly enhanced by the envelope function. This part of the radiation pattern gives rise to the main Cerenkov radiation lobe which is usually the one nearest to the direction of travel of the charged particle beam. As η increases the envelope function narrows about the Cerenkov angle and increases in height with the result that a single radiation lobe becomes increasingly dominant. In the limit of infinite path length, the radiation has only a single delta function like lobe centered at the Cerenkov angle.

Fig 1 and Fig 2 show radiation patterns for several different path lengths for 100 MeV electrons propagating in air. Taking the microwave value of the index of refraction to be $n=1.000268$ gives $n\beta=1.000255$, placing the peak of the envelope function at the Cerenkov angle of $\theta_c=1.3^o$. Fig 1 is calculated for $\eta=10$ and 20; Fig 2 for $\eta=150$, 250 and 1000. All the curves show a main peak and one or more subsidiary peaks, and the narrowing and growth in intensity with increasing path length described above.

In the Cerenkov case, $\sin^2 u$ is identically zero at the Cerenkov angle. Other zeroes occur when $u=m\pi$, where m is an integer. The set of angles at which sin u vanishes has already been given by (12) with the previously defined angles of θ_b, θ_c, and θ_a corresponding to m=+1, 0, and -1 respectively. The set continues with positive and negative m values for which $|\cos\theta_m| \leq 1$.

In order to have a small maximum precede the principle radiation lobe, another angle at which sin u vanishes must exist between $\theta=0$ and $\theta=\theta_a$. That is, the angle corresponding to a further negative m value must become physical. Setting $\theta_m=0$ gives a condition on the path length for addtional minor maxima.

$$\eta = m \frac{n\beta}{1 - n\beta} \tag{30}$$

For $n\beta>1$, the denominator in (30) is negative which in combination with a negative m value gives a positive result for η.

The next negative value is m=-2 so that (30) with that value of m should give an η value leading to a minor radiation lobe preceding the major one. Using $n\beta=1.02$ and m=-2 in (30) gives a path length of $\eta=102$ at which the minor lobe between $\theta=0$ and θ_c is evident.

Fig 9 is a plot of the radiation distribution for 100 MeV electrons traveling in a medium for which the index of refraction is n=1.020013. This unrealistically large index for a gas gives $n\beta=1.02$ as in Fig 6-8. The solid curve, calculated for $\eta=102$, shows a small peak preceding the principal one with a ratio of

peak heights of ~ 66. The dotted line, calculated for a beam length half as long (η=51), does not show such a peak.

For the same electrons in air, the lower index of air requires a longer path length of η=7846 at which the minor peak becomes apparent. Calculations confirm this, as well as showing other minor peaks when the path lengths found by substituting larger negative m values into (30) are attained.

DISCUSSION

The body of this paper is concerned with the production of radiation by a charged particle beam in which both the path length and the size of an individual charge bunch are finite. The effects of the size and shape of an individual charge bunch enter only through a multiplicative form factor and do not cause the radiation to spread in angle, or modify the threshold. Thus our main point is that the beam path length parameter η affects the production of radiation by a charged particle beam. The spatial pattern of the radiation, its intensity, and the beam energy necessary for producing Cerenkov or psuedo-Cerenkov radiation are dependent on η. The complimentary diffraction and envelope forms both describe these effects, with the latter giving a more direct description of the development of the radiation patterns in the sub-Cerenkov case.

Although $n\beta$ determines the position of the Cerenkov angle, the value of η controls the broadening of all the radiation lobes. Since the peak of the main lobe occurs in the vicinity of the peak of the Cerenkov envelope its height also depends on η. In the sub-Cerenkov case, $n\beta$ determines the position and height of the envelope and the change from psuedo-Cerenkov radiation to a rapidly oscillating one is dependent on η.

A distinguishing feature of Cerenkov radiation is the dramatic increase of intensity of the main radiation lobe with an increase in beam length as shown in Fig. 1, Fig. 2, and Fig. 9. In these figures, the ratios of the peak heights is very nearly equal to the square of the ratio of beam length parameters, after

the different positions of the peaks is taken into account. In contrast, in the sub-Cerenkov regime, the height of the radiation peaks is bounded by the finite height of the envelope function as shown in Fig. 7 and Fig. 8.

In a medium with a large index of refraction, such as water, the main radiation lobe occurs at a rather large angle to the beam and the lobe broadening subsides quickly for η values greater than 20. In addition, the dependence of the threshold energy on η is small. Contrarily, in a medium with an index close to one, such as a gas, the effect of η is more pronounced. The lobe broadening persists in variation of η over several decades before approaching the (much smaller) infinite path length limit of θ_c. Accompanying this behaviour, the threshold energy also varies over several decades of η so that the onset of radiation as a function of beam energy is not a sudden phenomena.

These effects are most apparent at small values of η (~10) and are of interest when observing microwave radiation produced from an RF linac. Although a high energy, high intensity charged particle beam may be shielded by a plasma sheath, Cerenkov radiation and the associated broadening of the main lobe as a result of a short beam length may arise from the regions at the ends of the beam.

Small radiation maxima may exist closer to the direction of travel of a charged particle beam than the major lobe. In the sub-Cerenkov case, the minor maxima occur when η increases so that the psuedo-Cerenkov regime goes over to the rapidly oscillating one. Appearance of the minor maxima depends on $n\beta$ as

well as η. For gases, n is slightly larger than 1, and an upper limit for β is also 1 so that a realistic upper limit is $n\beta=1.001$. This limit leads to $\theta_c=2.6^o$, and $\eta=2000$ in order to have a minor maxima precede the main lobe; values not very different from those found for 100 MeV electrons in air. In a denser medium the situation is different. In water where $\theta_c=41^o$, a value of $\eta=8$ would be sufficient to ensure that a leading minor maxima occur. Larger η values would have the possibility of producing a Cerenkov radiation pattern with many minor maxima preceding the main one.

In media with index of refraction near 1, the radiation described here has the same spatial characteristics as transition radiation . If the index is set equal to 1, the peak of the radiation envelope occurs at $\cos \theta_s=\beta$. Then $\sin \theta_s=\gamma^{-1}$, or for small θ_s, $\theta_s=\gamma^{-1}$ which is a characteristic of transition radiation.

As a final remark, it might be argued that the emission occuring below the usual Cerenkov threshold should not be named sub or pseudo-Cerenkov. But the argument in favor of retaining this name is that the radiation has a similar spatial appearance, the same polarization as Cerenkov radiation, and the transition to Cerenkov radiation as the energy is increased is smooth and continuous.

ACKNOWLEDGEMENT

This work was supported by the Naval Sea Systems Command and the Defense Advanced Research Projects Agency.

REFERENCES

1. F. R. Buskirk and J. R. Neighbours, Phys Rev A28, 1531-38 (1983).

2. John R. Neighbours, Fred R. Buskirk and A. Saglam, Phys Rev A29, 3246-52 (1984).

3. X. K. Maruyama, J. R. Neighbours, F. R. Buskirk, D. D. Snyder, M. Vujaklija, and R. G. Bruce, J Appl Phys 60(2) 518 (1986).

4. J. R. Neighbours and F. R. Buskirk, US Naval Postgraduate School Report No. NPS 61-84-010, 1984 (unpublished).

5. Fred R. Buskirk and John R. Neighbours, US Naval Postgraduate School Report No. NPS 61-84-007, 1984 (unpublished).

6. A. P. Kobzev, Yad. Fiz. 27, 1256 (1978) [Sov. J. Nucl. Phys. 27, 664 (1978)].

7. A. P. Kobzev and I. M. Frank, Yad. Fiz. 31, 1253 (1980) [Sov. J. Nucl. Phys. 31, 647 (1980)], and Yad. Fig. 34, 125 (1981) [Sov. J. Nucl. Phys 34, 71 (1981)].

8. A. Bodek, et al, Z. Physics C 18, 299 (1983)

9. X. K. Maruyama, J. R. Neighbours and F. R. Buskirk, IEEE Transactions on Nuclear Science NS-32, 1994 (1985).

FIGURE CAPTIONS

Fig 1. Calculated radiation intensity as a function of angle for an electron beam with a path length of 105 cm issuing from an S-band, 100 MeV linac into air (n = 1.000268). The solid curve is the pattern for radiation emitted at the fundamental frequency of 2.85 GHz so that the beam length parameter η has a value of 10. The dashed curve is the pattern for radiation emitted at the first harmonic frequency (η=20).

Fig 2. Calculated radiation intensity as a function of angle for an electron beam issuing from an S-band, 100 MeV linac for longer beam path lengths. The dotted, dashed and solid curves are for electron beam path lengths of 1574 cm, 2624 cm and 10496 cm respectively. The corresponding η values are 150, 250, and 1000.

Fig 3. First diffraction lobe angular limits θ_b and θ_a as a function of beam length parameter η for 100 MeV electron bunches traveling in air and water (n=1.333). The lower limit θ_a goes to zero at the beam length parameter value ηa. The dashed curve marked θ_m is the calculated angular value at which the peak of the main lobe occurs. (Values were obtained from the calculations leading to Fig 7 of Reference 2).

Fig 4. Threshold value of $n\beta$ as a function of beam length η. Values of $n\beta>1$ give rise to Cerenkov for all values of η. A value of $n\beta<1$, but above the curve gives rise to pseudo-Cerenkov radiation.

Fig 5. Threshold electron bunch energies as a function of η for water ($n=1.333$), air ($n=1.000268$) and helium ($n=1.000036$). At large values of η each curve approaches its respective E_T.

Fig 6. Envelope function $(G(n\beta,\theta))^2$ as a function of angle. The solid curve (Cerenkov) is for $n\beta=1.02$. The dashed curve (sub-Cerenkov) is for $n\beta=0.98$.

Fig 7. Sub-Cerenkov radiation patterns calculated for $n\beta=0.98$. The solid curve, calculated for $\eta=12$ is an example of psudeo-Cerenkov radiation. The dotted curve, calculated for $\eta=37$ shows a minor maxima preceding the largest lobe and a maxima of nearly the same intensity following it.

Fig 8. Rapidly oscillating sub-Cerenkov radiation pattern calculated for $n\beta=.98$ and $\eta=100$. Two minor maxima precede the largest lobe.

Fig 9. Cerenkov radiation patterns calculated for 100 MeV electron bunches traveling in a medium with an index of refraction of $n=1.020013$ and thus giving $n\beta=1.02$. The dotted curve is for $\eta=51$. The solid curve for $\eta=102$ shows a minor maxima preceding the principal radiation lobe.

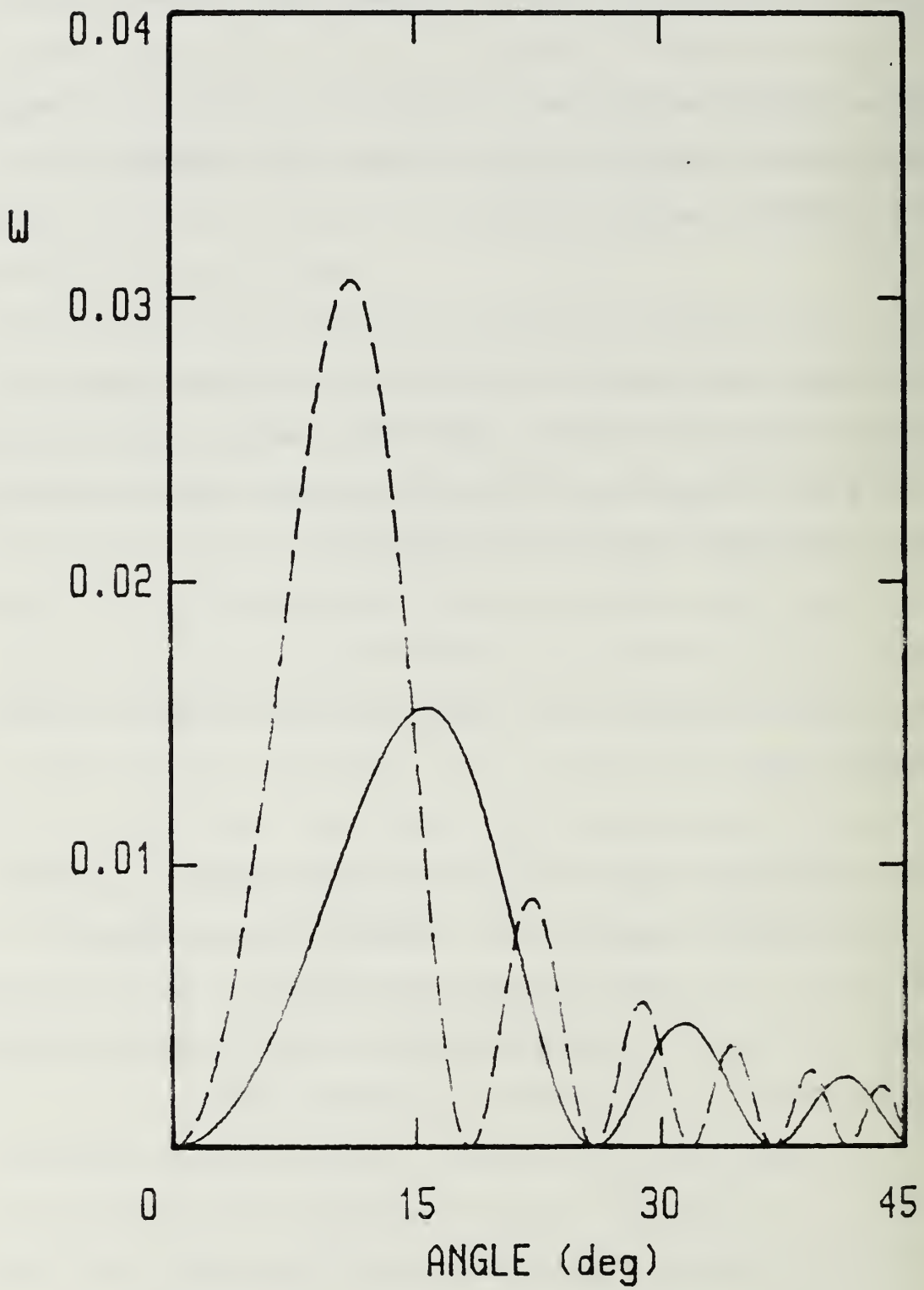
0.04
W
0.03
0.02
0.01
0
15
30
45
ANGLE (deg)

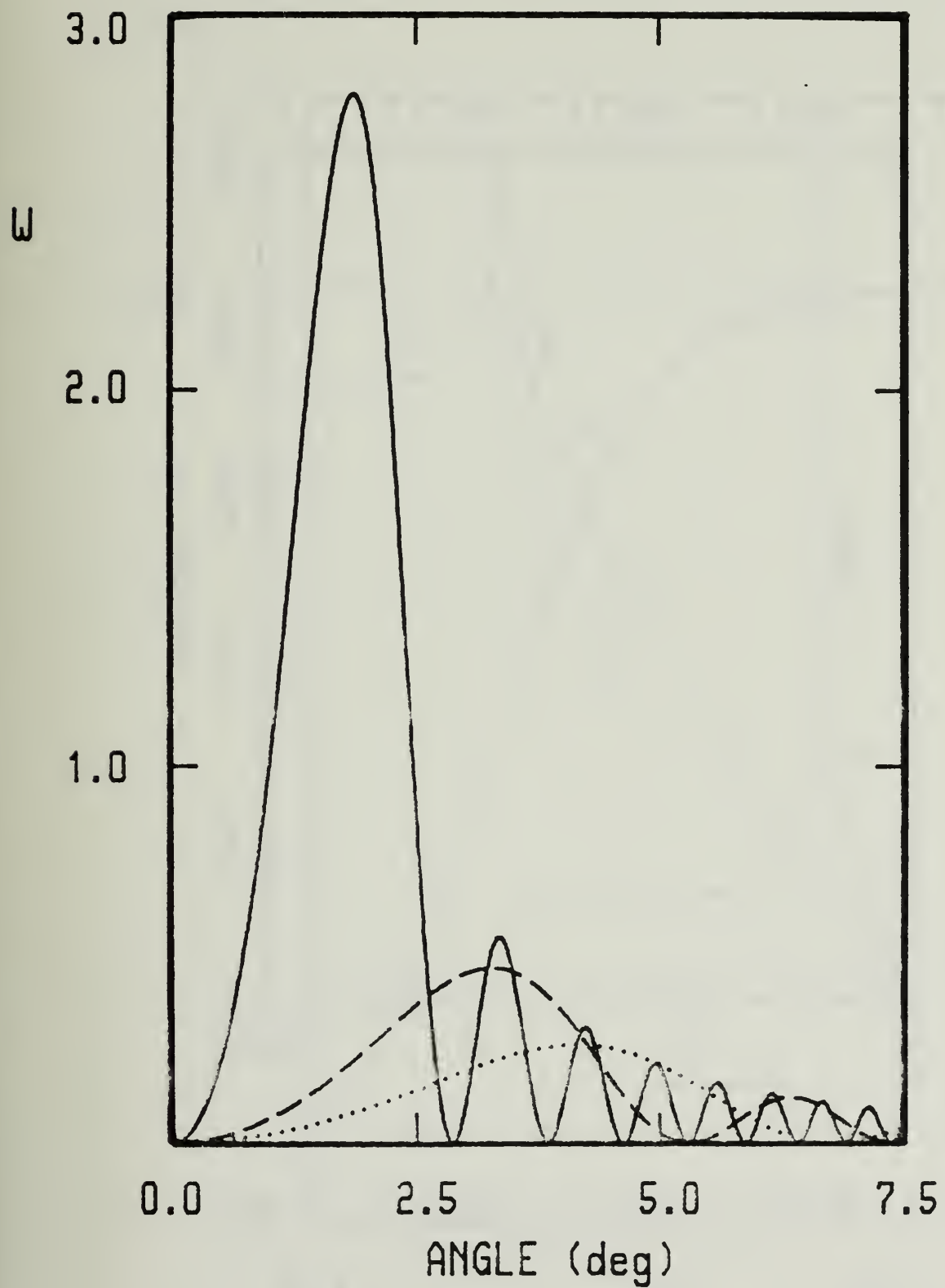
3.0
W
2.0
1.0
0.0
2.5
5.0
7.5
ANGLE (deg)

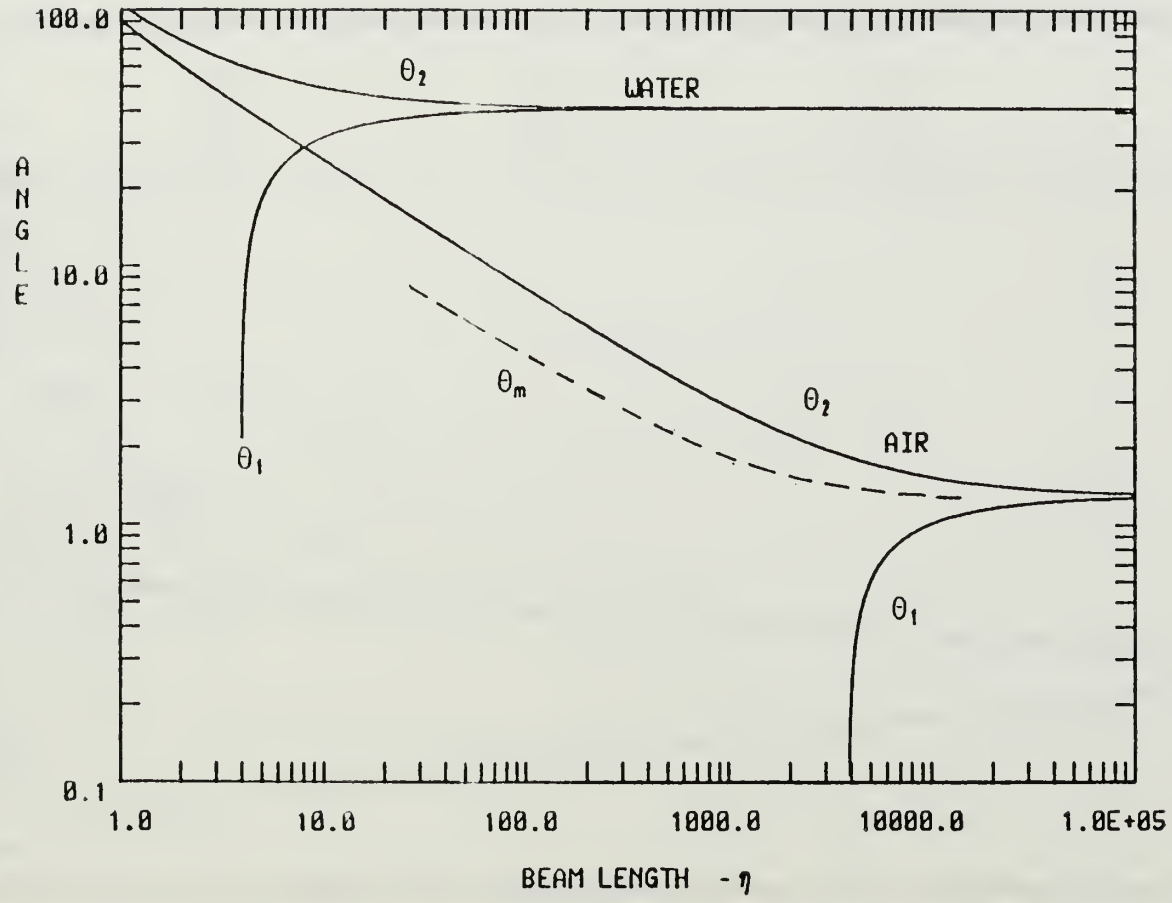
100.0
10.0
1.0
0.1
ANGLE
θ_2
WATER
θ_m
θ_2
AIR
θ_1
θ_1
1.0
10.0
100.0
1000.0
10000.0
1.0E+05
BEAM LENGTH - η

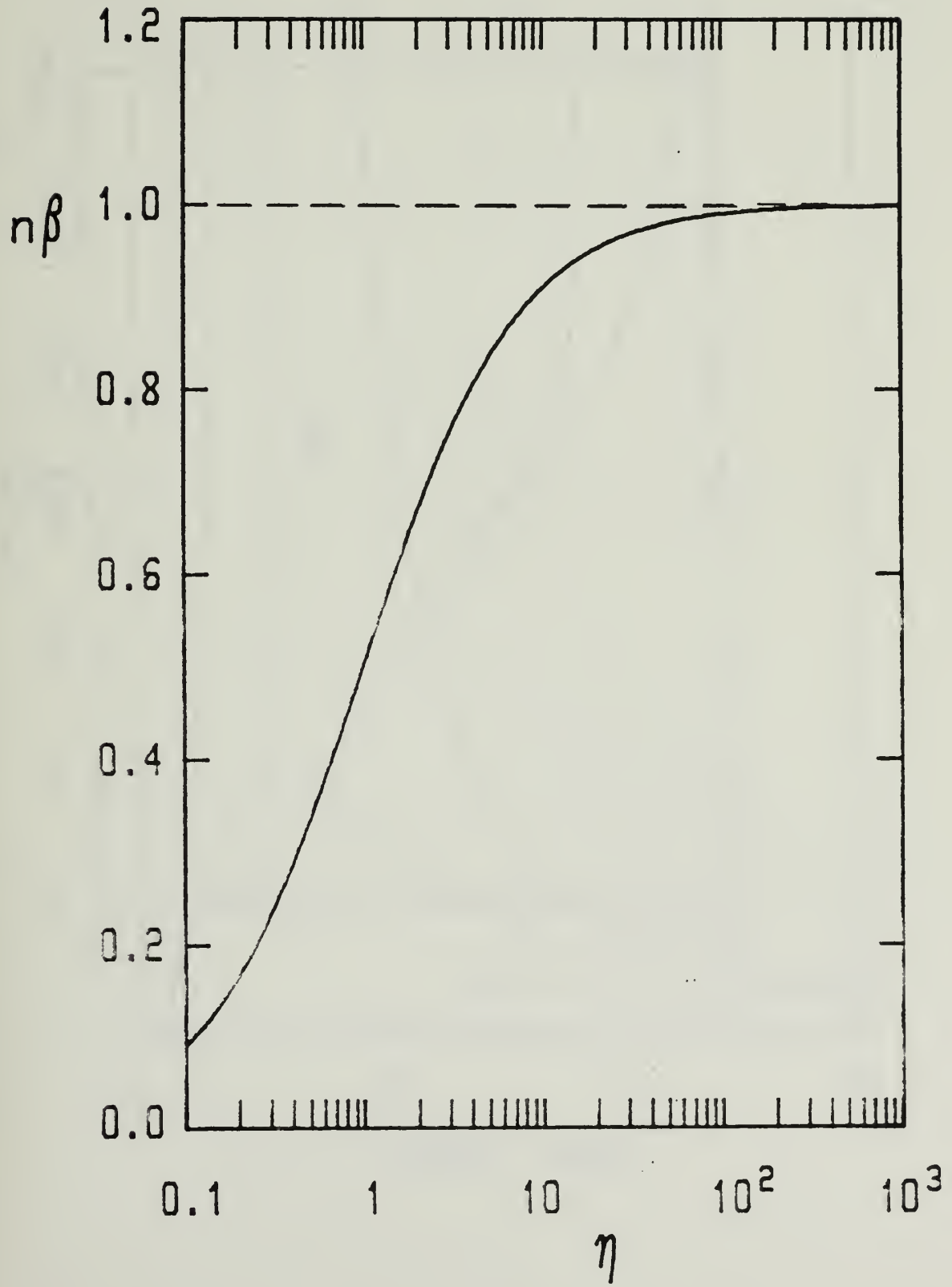
1.2
1.0
0.8
0.6
0.4
0.2
0.0
nβ
0.1
1
10
10²
10³
η

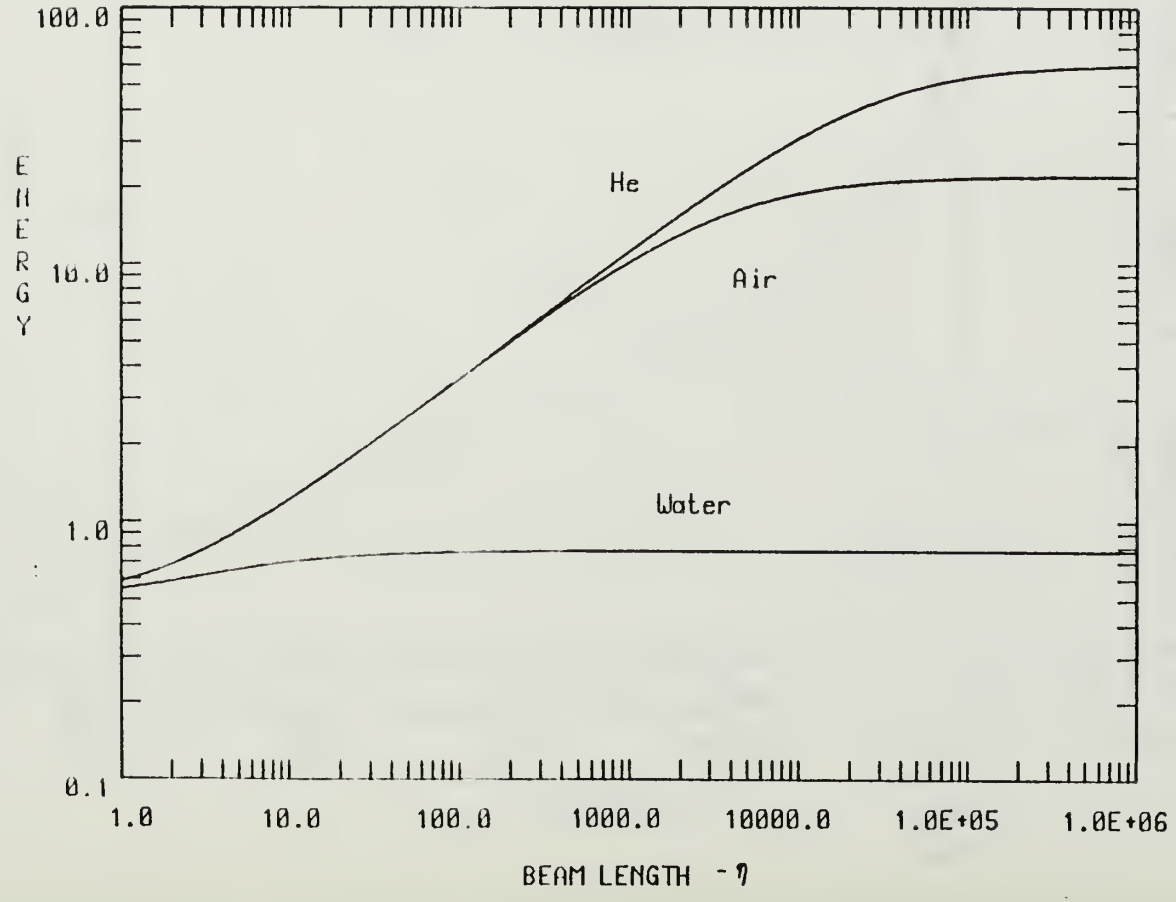
100.0
10.0
1.0
0.1
ENERGY
He
Air
Water
1.0
10.0
100.0
1000.0
10000.0
1.0E+05
1.0E+06
BEAM LENGTH - η

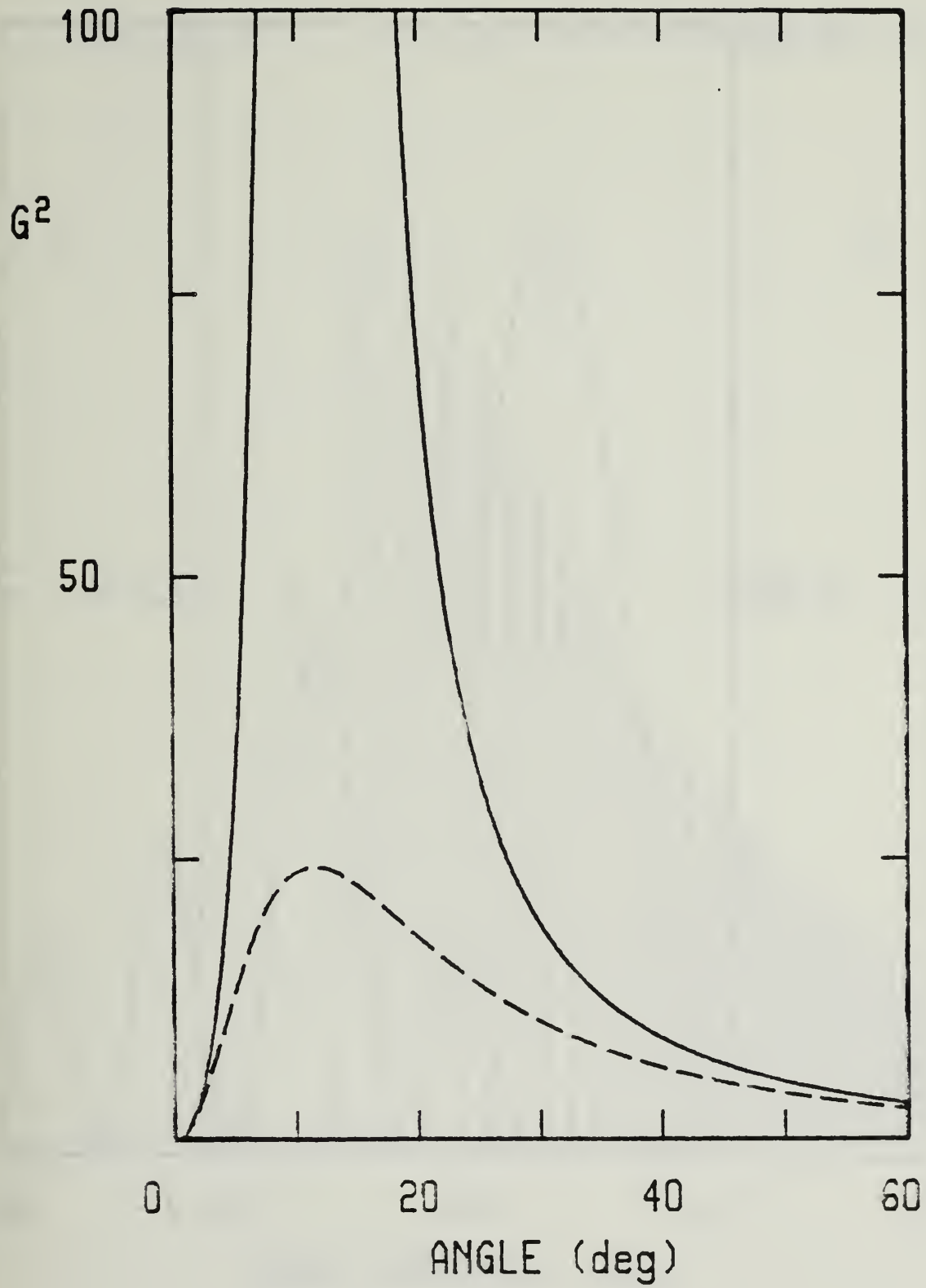
100
G^2
50
0
20
40
60
ANGLE (deg)

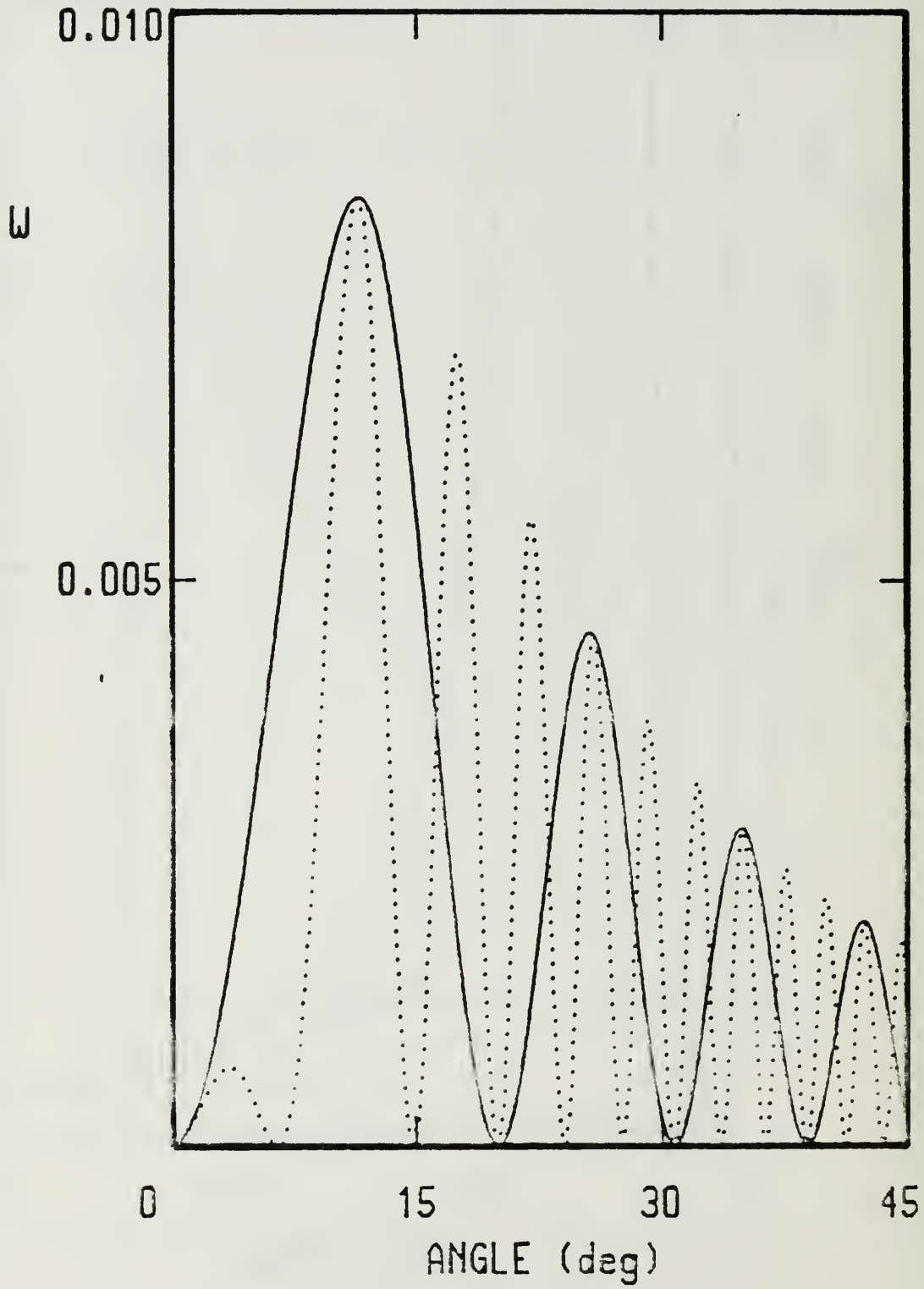
0.010
W
0.005
0
15
30
45
ANGLE (deg)

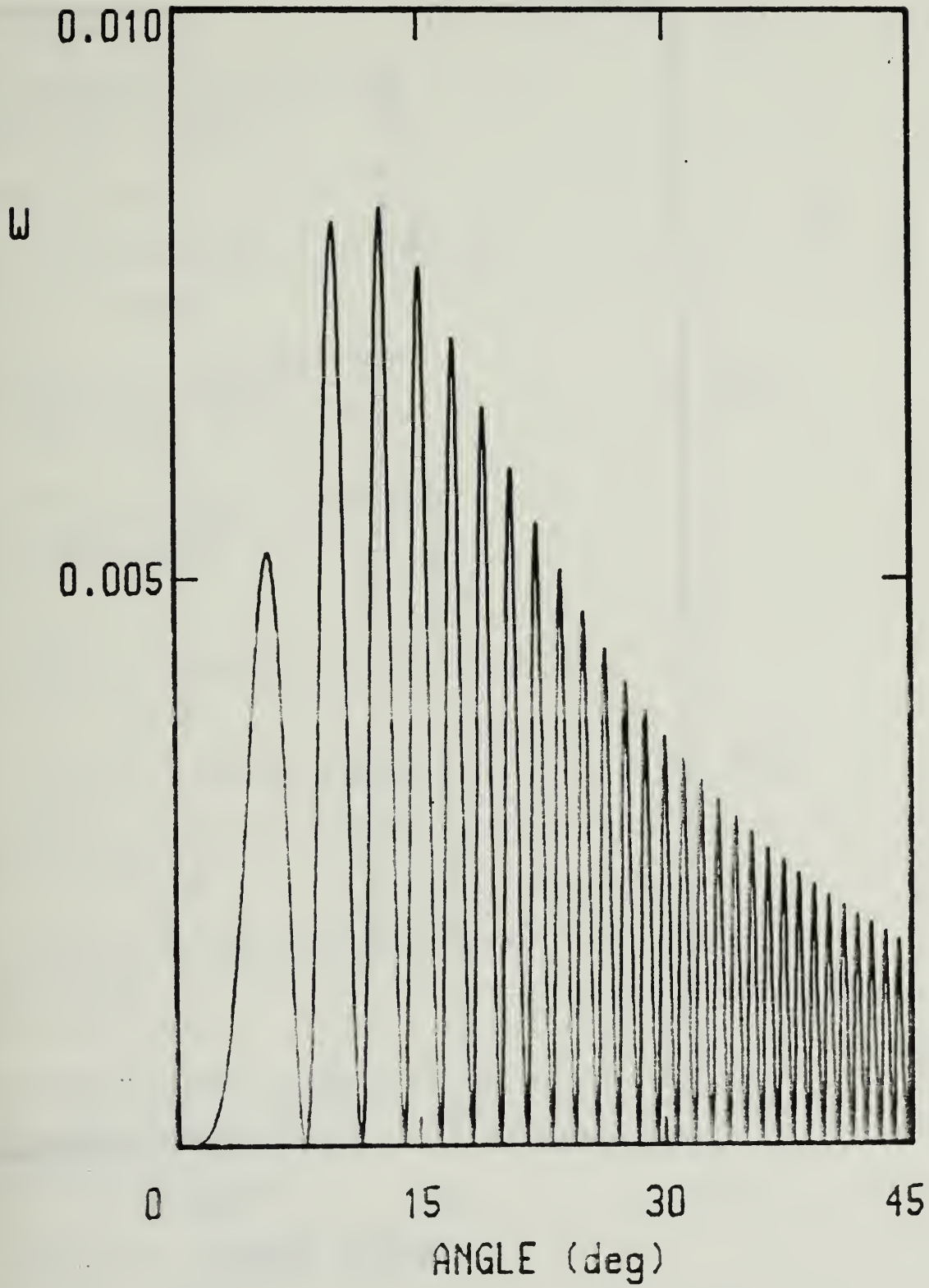
0.010
W
0.005
0
15
30
45
ANGLE (deg)

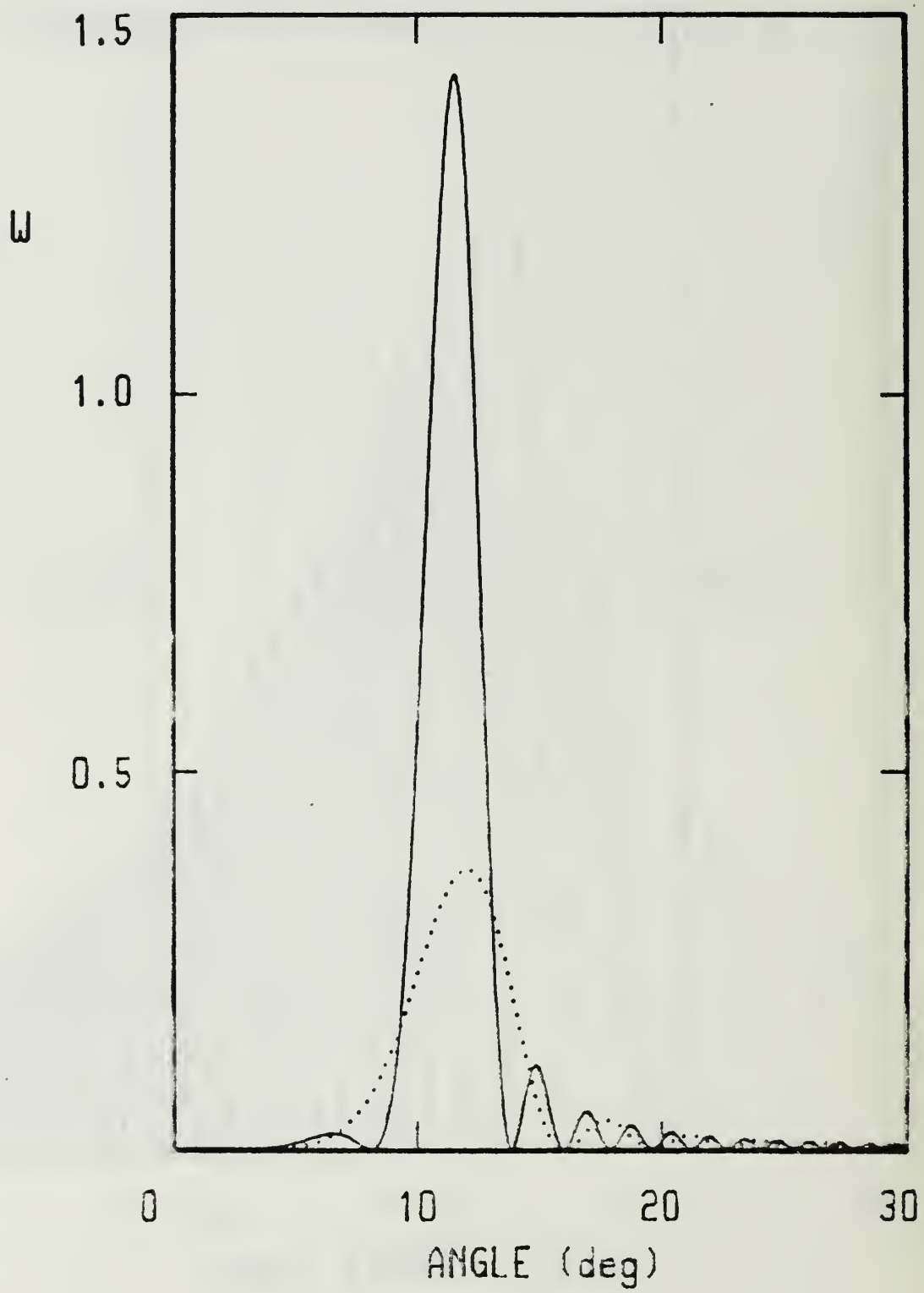
1.5
W
1.0
0.5
0
10
20
30
ANGLE (deg)

DISTRIBUTION LIST

CDR William Bassett — 1
PMS 405
Strategic Systems Project Office
Naval Sea Systems Command
Washington, D.C. 20376

Dr. Richard Briggs — 2
L-321
Lawrence Livermore National Laboratory
Box 808
Livermore, CA 94550

F. R. Buskirk & J. R. Neighbours — 20
Naval Postgraduate School
Physics Department, Code 61
Monterey, CA 93943

The Charles Stark Draper Laboratory — 1
ATTN: Dr. Edwin Olsson
555 Technology Square
Cambridge, MA 02139

Dr. W. Colson — 1
Berkeley Research Associates
P. O. Box 241
Berkeley, CA 94701

Director, Defense Advanced Research — 2
Project Agency
ATTN: LCOL Richard A. Gullickson
1400 Wilson Blvd.
Arlington, CA 22209

Defense Advanced Research Project Agency — 1
ATTN: MAJ George P. Lasche
1400 Wilson Blvd.
Arlington, VA 22209

Defense Advanced Research Projects Agency — 1
ATTN: Dr. Shen Shey
Directed Energy Office
1400 Wilson Boulevard
Arlington, VA 22209-2308

Defense Technical Information Center — 2
Cameron Station
Alexandria, VA 22314

Directed Technologies 2
ATTN: Mr. Ira F. Kuhn, Jr.
Dr. Nancy J. Chesser
1226 Potomac School Road
McLean, VA 22101

Dr. Luis Elias 1
Physics Department
UCSB
Santa Barbara, CA 93106

Dr. K. Felch 1
Varian Corporation
611 Hansen Way
Palo Alto, CA 94303

Dr. V. L. Granatstein 1
Electrical Engineering Dept.
University of Maryland
College Park, MD 20742

Dr. C. M. Huddleston 1
ORI, Inc.
1375 Piccard Drive
Rockville, MD 20850

Lawrence Berkeley Laboratory 1
ATTN: Dr. Edward P. Lee
Building 47, Room 111
1 Cyclotron Road
Berkeley, CA 94720

Lawrence Livermore National Laboratory 10
University of California
ATTN: Dr. William A. Barletta
Dr. Daniel S. Prono
Dr. Adrian C. Smith
Dr. Simon S. Yu
Dr. John T. Weir
Dr. Thomas J. Karr
Dr. William M. Fawley
Dr. Eugene J. Lauer
Dr. George J. Caporaso
Ms. Lois Barber
P. O. Box 808
Livermore, CA 94550

Library 2
Code 0142
Naval Postgraduate School
Monterey, CA 93943

Los Alamos National Laboratory 4
ATTN: Dr. Randolph Carlson
Dr. S. Szuchlewski
Dr. J. M. Mack
Ms. Leah Baker
Mail Stop P940
P. O. Box 1663
Los Alamos, NM 87545

Dr. Joseph Mack 1
M4, M.S. P-940
Los Alamos National Laboratory
Los Alamos, NM 87545

Dr. J. Madey 1
Department of Physics
Stanford University
Stanford, CA 94305

Prof. T. C. Marshall 1
Dept. of Applied Physics and
Nuclear Engineering
Columbia University
New York, NY 10027

Dr. Xavier K. Maruyama 1
Bldg. 245, Room R-108
National Bureau of Standards
Gaithersburg, MD 20899

Dr. David Merritt 1
PMS 405
Strategic Systems Project Office
Naval Sea Systems Command
Washington, D.C. 20376

Mission Research Corporation 1
ATTN: Dr. N. J. Carron
P. O. Box 719
Santa Barbara, CA 93102

Mission Research Corporation 2
ATTN: Dr. Brendan B. Godfrey
Dr. Dushan Mitrovitch
Plasma Sciences Division
1720 Randolph Road, SE
Albuquerque, NM 87106

Naval Research Laboratory 5
ATTN: Dr. Martin Lampe (4790)
Dr. A. Wahab Ali (4700.1)
Dr. Donald Murphy (4760)
Dr. Richard Fernsler (4770)
Dr. Glen Joyce (4790)
4555 Overlook Avenue, SW
Washington, D.C. 20375

Naval Surface Weapons Center 9
White Oak Laboratory
ATTN: Dr. Eugene E. Nolting (R401)
Dr. Andy Smith (H23)
Ms. Beverly McLean (R401)
Dr. H. C. Chen (R41)
Dr. Han S. Uhm (R41)
Dr. Ralph Fiorito (R41)
Dr. John Smith (R41)
Dr. Donald Rule (R41)
Dr. M. J. Rhee (R41)
10901 New Hampshire Avenue
Silver Springs, MD 20903-5000

Office of Research Administration 1
Code 012
Naval Postgraduate School
Monterey, CA 93943

Dr. C. Pellegrini 1
Brookhaven National Laboratory
Bldg. 902
Accelerator Dept.
Upton, NY 11973

Sandia National Laboratories 5
ATTN: Dr. Carl Ekdahl (1272)
Dr. Ron Lipinski
Dr. Michael Mazarakis (1272)
Dr. John Freeman (1241)
Dr. Gordon T. Leifeste (1272)
P. O. Box 5800
Albuquerque, NM 87185

Science Applications International Corp. 5
ATTN: Dr. Robert Johnston
Dr. R. Leon Feinstein
Dr. R. Richardson
Dr. Douglas Keeley
Dr. C. Yee
5150 El Camino Real, Suite B-31
Los Altos, CA 94022

SRI International 1
ATTN: Dr. Donald J. Eckstrom
333 Ravenswood Avenue
Menlo Park, CA 94025

CAPT. Kurt Stevens 1
AFTAC/TX OP
Patrick AFB
Patrick, FL 32925

Dr. Kenneth Struve
Lawrence Livermore National Labratory
P. O. Box 808
Livermore, CA 94550

Admiral R. L. Topping 1
Space and Naval Warfare Systems Command
SPAWAR-06
Washington, DC 20363-5100

LCDR E. Turner 1
PMS 405
Strategic Systems Project Office
Naval Sea Systems Command
Washington, DC 20376

Dr. R. Warren 1
Los Alamos Scientific Laboratory
P. O. Box 1663
Los Alamos, NM 87545

MAJ Edward Pogue 1
SD10-DE
Pentagon
Washington, DC 20301-7100

DUDLEY KNOX LIBRARY
3 2768 00337458 8